Journal of Photochemistry and Photobiology A: Chemistry 221 (2011) 30–37

Contents lists available at ScienceDirect

Journal of Photochemistry and Photobiology A: Chemistry

journal homepage: www.elsevier.com/locate/jphotochem

Photochemical synthesis of copper sulphide/titanium oxide photocatalyst

Luminita Andronic*, Luminita Isac, Anca Duta*

The Centre: Product Design for Sustainable Development, Transilvania University of Brasov, Eroilor 29, 500036, Brasov, Romania

ARTICLE INFO

Article history:
Received 30 January 2011
Received in revised form 4 April 2011
Accepted 9 April 2011
Available online 16 April 2011

Keywords:
Photochemical synthesis
Copper sulphide
Titanium oxide
Photocatalysis
Methyl orange
Methylene blue

ABSTRACT

Copper sulphide powder was obtained by the photochemical synthesis and thin films were developed by doctor blade deposition of Cu_xS and Cu_xS/TiO_2 composites with photocatalytic properties. The photochemical process could be adjusted to prepare Cu_xS with different photocatalytic activities by changing the $CuSO_4$:$Na_2S_2O_3$ molar ratio while keeping other conditions unchanged (solutions pH, solutions volume, irradiation time and intensity). The powder and thin film properties were characterized in terms of: the Fourier transform infra-red (FTIR), the X-ray diffraction (XRD), UV–vis spectroscopy, atomic force microscopy (AFM).

The photocatalytic process using Cu_xS and coupled Cu_xS/TiO_2 thin film semiconductors in the dyes photodegradation (methyl orange and methylene blue) was investigated. The photocatalytic activity of Cu_xS/TiO_2 nanocomposites depends on the Cu_xS:TiO_2 ratio; the best results correspond to the Cu_xS/TiO_2 (Cu_xS:TiO_2 = 3:7) photocatalysts, with high efficiency (almost 99%) after 300 min for methyl orange, respectively after 180 min for methylene blue degradation, under UV irradiation, when H_2O_2 is added in photocatalytic process. The semiconductors association and the films homogeneity limit the electron–hole recombination, resulting in good efficiency in dyes photodegradation even under visible light irradiation.

1. Introduction

Photocatalytic degradation is an advanced oxidation process which can develop as a promising technology for treating wastewaters with complex organic pollutants load, as there are those resulted in the textile finishing industry. Therefore, the photocatalytic degradation of dyes, using semiconductor films as photocatalysts has been extensively studied [1–3].

Among the materials developed for photocatalytic applications (TiO_2, ZnO, CdS, WO_3) [4–7], titanium dioxide (the anatase polymorph) is often referred to as the most promising material due to its high efficiency, low cost, chemical inertness, and photostability. The main drawback is its wide band gap (3.2 eV) which requires ultraviolet (UV) irradiation for photocatalytic activation, so any shift in the optical response of TiO_2, from UV to the visible spectral range will have a positive effect on the photocatalytic efficiency under solar irradiation and on industrial up-scaling [1].

The coupling of two semiconductors, possessing different energy levels for their corresponding conduction band (CB) and valence band (VB), can be used to enhance photocatalysis, in a binary system containing titanium oxide and a narrow band gap semiconductor [8]. Under visible light irradiation, composites containing Bi_2S_3/TiO_2 nanostructures were found to have good photocatalytic activity for dyes degradation [9] and MoS_2/TiO_2 and WS_2/TiO_2 nanostructures demonstrate to have high photocatalytic activity for methylene blue decomposition [10,11].

Copper sulphides were largely investigated in the recent years due to the interesting optical and electrical properties, resulted from the variations in stoichiometry, composition, morphology, and due to their potential applications in various fields: absorbers for solid state solar cells [12], room-temperature ammonia gas sensor [13], and photocatalytic reactions [14]. Stoichiometric and nonstoichiometric copper sulphides were often obtained as five crystalline polymorphs: chalcocite (Cu_2S), djurleite ($Cu_{1.95}S$), digenite ($Cu_{1.8}S$), anilite ($Cu_{1.75}S$) and covellite (CuS) [15–17].

Copper sulphide powders can be successfully synthesized by various wet techniques: solvothermal [18], hydrothermal [19], microemulsion [20] and photochemical methods [21].

The photochemical synthesis of copper sulphide powders, using $CuSO_4$ and $Na_2S_2O_3$ solutions [22], can be described by a set of concurrent reactions, involving electrons and/or proton transfer and the ionic species resulted from the precursors' dissociation. The copper salt is dissolved in distilled water forming, depending on pH, the $[Cu(H_2O)_{4\ldots6}]^{2+}$ ions [23]; in the working conditions, an equilibrium between the Cu(II) and Cu(I) oxidation states can also be expected.

$$Cu^{2+}(aq.) + Cu \Leftrightarrow 2Cu^{+}(aq.) \quad (1)$$

* Corresponding authors. Tel.: +40 741 264922.
E-mail addresses: andronic-luminita@unitbv.ro (L. Andronic), a.duta@unitbv.ro (A. Duta).

1010-6030/$ – see front matter © 2011 Elsevier B.V. All rights reserved.
doi:10.1016/j.jphotochem.2011.04.018

In aqueous solutions hydration occurs, along with many other possible processes, but the reactions mainly responsible for Cu_xS formation can be considered the following:

$$CuSO_4 \Leftrightarrow Cu^{2+} + SO_4^{2-} \quad (2)$$

$$Na_2S_2O_3 \Leftrightarrow 2Na^+ + S_2O_3{}^{2-} \quad (3)$$

$$S_2O_3^{2-} + h\upsilon \rightarrow S + SO_3^{2-} \quad (4)$$

$$2S_2O_3^{2-} + h\upsilon \rightarrow S_4O_6^{2-} + 2e^- \quad (5)$$

$$S_2O_3^{2-} + H^+ \rightarrow HSO_3^- + S \quad (6)$$

$$S + 2e^- \rightarrow S^{2-} \quad (7)$$

$$2Cu^{2+} + S + 4e^- \rightarrow Cu_2S \quad (8)$$

$$[Cu(H_2O)_{4\ldots6}]^{2+} + S + 2e^- \rightarrow CuS \cdot (H_2O)_x + (4\ldots6 - x)H_2O \quad (9)$$

$$[Cu(H_2O)_{4\ldots6}]^{2+} + S + 2e^- \rightarrow CuS + (4\ldots6)H_2O \quad (10)$$

$$2Cu^{2+} + 2S_2O_3^{2-} \Leftrightarrow Cu_2S + 3SO_2 \quad (11)$$

$$Cu^{2+} + S_2O_3^{2-} + H_2O \Leftrightarrow CuS + SO_4^{2-} + 2H^+ \quad (12)$$

The use of films in industrial processes is recommendable, avoiding the technological problems raised by powder leaching and separation. Therefore, Cu_xS powders were prepared by photochemical synthesis and immobilised as thin films using the doctor blade technique. Composite thin films were also prepared by mixing the copper sulphide in various ratios with TiO_2 (Degussa P25) powders. The efficiency of dyes (methyl orange and methylene blue) photodegradation using Cu_xS powders or films, single or coupled as Cu_xS/TiO_2 was further investigated under UV and under visible light irradiation.

2. Experimental

2.1. Materials

- Copper sulphate $CuSO_4 \cdot 5H_2O$, $M = 249.68$, Scharlau Chemie S.A.
- Sodium tiosulphate $Na_2S_2O_3 \cdot 5H_2O$, $M = 248.18$, Scharlau Chemie S.A.
- Triton X-100 (non-ionic surfactant) *t*-oct-C_6H_4–$(OCH_2CH_2)_nOH$, $n = 9$–10, $d = 1.070$, Scharlau Chemia S.A.
- TiO_2 Degussa P25, 80% anatase and 20% rutile; specific surface area 55 $m^2\,g^{-1}$ and a mean particle size of 25 nm
- Methyl orange, $C_{14}H_{14}N_3NaO_3S$, $M = 327.34$, E.Merck
- Methylene blue, $C_{16}H_{18}N_3SCl$, $M = 319.86$, Fluka AG, Buchs SG
- Hydrogen peroxide 30%, $M = 34.01$, $d = 1.11$ g/cm^3, Scharlau Chemia S.A.
- Microscopy glass, Heinz Herenz
- Sulphuric acid, Sigma–Aldrich

2.2. Photochemical synthesis of the copper sulphide powder

The copper sulphide powders were obtained by photochemical synthesis, using aqueous precursors' solutions. In a typical procedure, $CuSO_4$ 0.5 M was mixed with $Na_2S_2O_3$ 0.05 M to obtain 600 mL of precursors solution and the pH was adjusted at 3 by adding the H_2SO_4 conc. The reaction was carried out in a photocatalytic reactor with three F18W/T8 black light tubes (Philips) (UVA light, typically 340–400 nm, with $\lambda_{max} = 365$ nm), placed annular to the photoreactor. Copper sulphide samples (A1–A5) were obtained after 3 h of irradiation, at room temperature, using variable $CuSO_4$:$Na_2S_2O_3$ ratios (r): A1 ($r = 1$); A2 ($r = 5$); A3 ($r = 10$); A4 ($r = 20$); A5 ($r = 30$).

The resulted black precipitates were washed with bi-distilled water a few times, and filtrated (Millipore 0.45 μm filter), then they were dried in air. The final dark products were annealed for 3 h at 350 °C; the annealing temperature was selected considering the thermal stability of the compounds.

Fourier Transform Infrared Spectroscopy (FTIR, Spectrum BX Perkin Elmer) was used to record spectra in reflectance mode, from 500 to 4500 cm^{-1}, after 4 scans, with resolution of 4 cm^{-1}.

The phase structure of the powders was characterized by X-ray diffraction (XRD, Brucker D8 Discover diffractometer with CuKα radiation).

2.3. Thin films of Cu_xS and Cu_xS/TiO_2

Thin films of Cu_xS and Cu_xS/TiO_2 composites were obtained by doctor blade, using the copper sulphide powder which showed the best efficiency in dyes photo-degradation (sample A3), respectively TiO_2 Degussa P25.

For the doctor blade deposition of nanoporous thin films, an aqueous colloid paste is formed by mixing powder (0.5 g) with ethanol (4 mL), and surfactant Triton X100 (1 mL, 10%). The paste was homogenized for 10 min. Finally, the paste was smeared on glass substrate (1.5×2.5 cm^2) previously cleaned with ethanol, distilled water, acetone in successive sonication processes. After drying in air at 60 °C for about 2 min, the films were annealed in an oven at 350 °C for 3 h.

Different Cu_xS–TiO_2 nanocomposite films were prepared by varying the Cu_xS:TiO_2 weight ratio in the paste (1:9 in sample A3-1; 3:7 in sample A3-2; 1:1 in sample A3-3).

The photocatalytic activity of these films was compared with that corresponding to single component films, of TiO_2 respectively Cu_xS.

The UV–vis transmittance spectra of the Cu_xS and Cu_xS/TiO_2 composite thin films were recorded using a Perkin Elmer Lamda 25 spectrophotometer, and the energy band gaps were estimated.

The surface morphology and porosity was investigated by atomic force microscopy (AFM-NT-MDT model NTGRA PRIMA EC). The images were taken in semi-contact mode with "GOLDEN" silicon cantilever (NCSG10, force constant 0.15 N/m, tip radius 10 nm). Scanning was conducted on three different places (a certain area of 50×50 μm for each section) randomly chosen, at a scanning rate of 1 Hz. Image analysis was carried using WSxM software, to evaluate the pore size distribution [24].

2.4. Photocatalysis experiments

The activity of the copper sulphide powders was firstly examined in the photocatalytic bleaching of methyl orange (MO) solutions; this dye was selected being rather difficult to degrade due to a very stable structure.

The reactor used for the photochemical synthesis was also used in the photocatalytic experiments.

A suspension containing 0.1 g of the Cu_xS powder catalyst and 25 mL of MO solution (0.0125 mM) was magnetically stirred, and aliquots were taken each 60 min and filtrated (Millipore 0.45 μm filter) to remove the photocatalyst.

The photodegradation efficiency was evaluated using the following relation:

$$\eta = \frac{c_0 - c}{c_0} \cdot 100 \quad (13)$$

where c_0 represents the initial concentration and c represents the concentration at time t.

The photocatalytic activity of the Cu_xS and Cu_xS/TiO_2 composite films (sample of 1.5×2.5 cm^2) were evaluated in the methyl orange and methylene blue (MB) photodegradation. The results were compared with those previously reported on TiO_2 Degussa P25 thin films [25]. The effect of the initial dyes concentration (0.05–0.003125 mM), of the irradiation time (0–360 min), and of

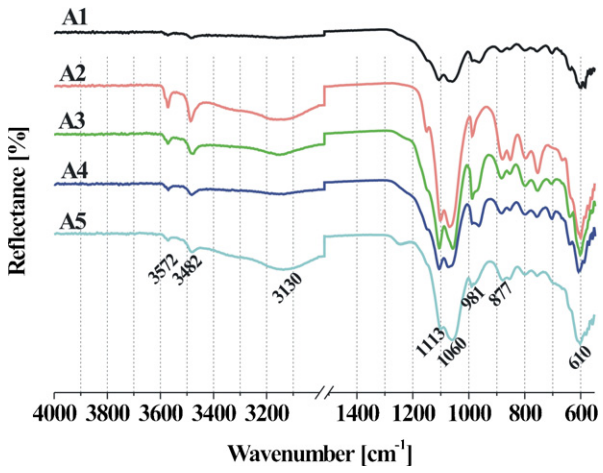

Fig. 1. FT-IR analysis of the copper sulphide powders.

the electron acceptor (H_2O_2 30%, 4 mL/L dye solution) were investigated and the optimised process conditions were identified.

For comparison, blank samples containing only MO or MB without photocatalyst, were subjected to UV irradiation in the photocatalytic reactor. The MO dye proved to be highly stable to photolysis while MB solutions exhibited low degradation.

Considering the optimized UV photodegradation conditions, similar experiments were developed under VIS irradiation, to investigate the ability of the composite films for sun-induced wastewater treatment applications.

In all experiments, the initial and the residual dye's concentration were evaluated using a spectrophotometer (Perkin Elmer Lambda 25) at the maximum absorption wavelength (463 nm for MO respectively 665 nm for MB), experimentally registered, using the calibration curve.

The photocatalytic degradation kinetics of methyl orange and methylene blue using Cu_xS/TiO_2 composite thin films were also analyzed.

3. Results and discussion

3.1. Chemical and phase composition of the Cu_xS powder

The Fourier transform infra-red (FTIR) and the X-ray diffraction (XRD) analysis were used to characterize the copper sulphide powder samples.

The chemistry of sulphide-containing particles was studied by IR spectrometry. The most intensive bands were found in the intervals 584–731, 835–1046, 1094–1264 cm^{-1} (Fig. 1).

According to the literature data [26], the peaks were assigned to the symmetric valence S–S vibrations ν_s(S–S), to the symmetric deformation O–S–O vibrations, to the symmetric valence S–O vibrations δ_s(O–S–O), and to the asymmetric valence S–O vibrations ν_s(S–O), as presented in Table 1. The SO_4^{2-} anions produce characteristic infrared bands at 614 cm^{-1} and 1064 cm^{-1} (Table 1). The copper sulphate contains two types of groups of hydrogen bonding: the water molecules that are incorporated into the lattice structure of $CuSO_4$ precursor produce characteristic sharp bands at 3104 cm^{-1} and the O–H bonding (1670 cm^{-1}) (Fig. 1).

These data show that beside copper sulphides, the samples also contain by-products of the photochemical reactions as presented in Eqs. (1)–(12): sulphates, sulphites, tetrathionates, or unreacted tiosulphate, or can be form during the calcinations of the final product.

The variation of the chemical composition of the crystalline phases in the powders was examined by X-ray diffraction, as presented in Fig. 2.

The diffraction patterns of A1, A3 respectively A5 samples show numerous peaks corresponding to sulphides (copper and sodium) and to the unreacted precursors ($CuSO_4$, $Na_2S_2O_3$), their correspondence in XRD pattern is: (1) CuS Covellite (JCPDS: 06-0464, (2) $Cu_{1.8}S$ Digenite (JCPDS: 47-1748), (3) $Cu_{1.75}S$ Roxybite (JCPDS: 23-0958), (4) $Cu_{1.81}S$ (JCPDS: 41-0959), (5) $Cu_{1.8}S$ Digenite (JCPDS: 26-0476), (6) Cu_2S (JCPDS: 12-0175), (7) $Cu_{1.92}S$ (JCPDS: 30-0505), (8) $CuSO_4$ (JCPDS: 14-0373), (9) Cu_2SO_4 (JCPDS: 28-0401), (10) $Na_2S_2O_3$ (JCPDS: 02-0277 (11) Na_2S_3 (JCPDS: 44-0822), (12) Cu_2S chalcocite, (JCPDS: 12-0227). A mixture of sulphites was also previously obtained in photochemical deposition by Podder et al. [22].

Compositions having the $CuSO_4$:$Na_2S_2O_3$ ratios above 1 show an improved crystallinity and the predominant formation of $Cu_{1.8}S$ but, as expected the powders consist of copper sulphides (43.7–72.5%) and a variable amount of by-products (Table 2).

This can explain the rather poor results obtained in the MO photocatalytic degradation: it can be concluded that the sample A1 has a lower photocatalytic activity, possible due to the lower amount of crystalline phase and due to the CuS composition, less active. Unreacted copper sulphate was found in the A4 and A5 samples also leading to low efficiencies. The best results correspond to the A3 sample, having a quite large copper excess in the precursor solution, and this was selected for further thin films deposition.

3.2. The optical properties of the Cu_xS/TiO_2 composite films

The photocatalytic activity of catalyst is influenced by the optical properties of the films, especially of the band gap energy value.

Copper sulphide as bulk material shows both an indirect band gap between 1.05 and 1.21 eV [27] and a direct gap between 2.4 and 2.36 eV [28].

Optical absorption and transmittance measurements have been carried out to calculate the band gap of the Cu_xS/TiO_2 composite films. The optical absorption band gap E_g can be estimated using the following formula [29]:

$$\alpha h\upsilon = A(h\upsilon - E_g)^n \quad (14)$$

where α is a constant, $h\nu$ is the photon energy, E_g is the semiconductor band gap energy and n is a constant ($n = 1/2$ for a direct gap and

Table 1
Wavenumber of the characteristic peaks of Cu_xS powder samples.

Sample	Wavenumber [cm^{-1}]												
	ν_{as} (S–O)	ν_{as} (S=O)	ν_s(S–O)				δ_s(O–S–O)						ν_s(S–S)
A1	1106	1060	962	882	856	800	756	702	636	598	584	560	523
A2	1102	1068	988	880	852	796	754	–	–	600	–	–	523
A3	1106	1056	988	882	854	798	754	704	638	602	–	–	523
A4	1106	1072	964	882	854	798	756	702	636	608	–	558	523
A5	1100	1060	990	878	854	798	–	–	756	602	–	558	523

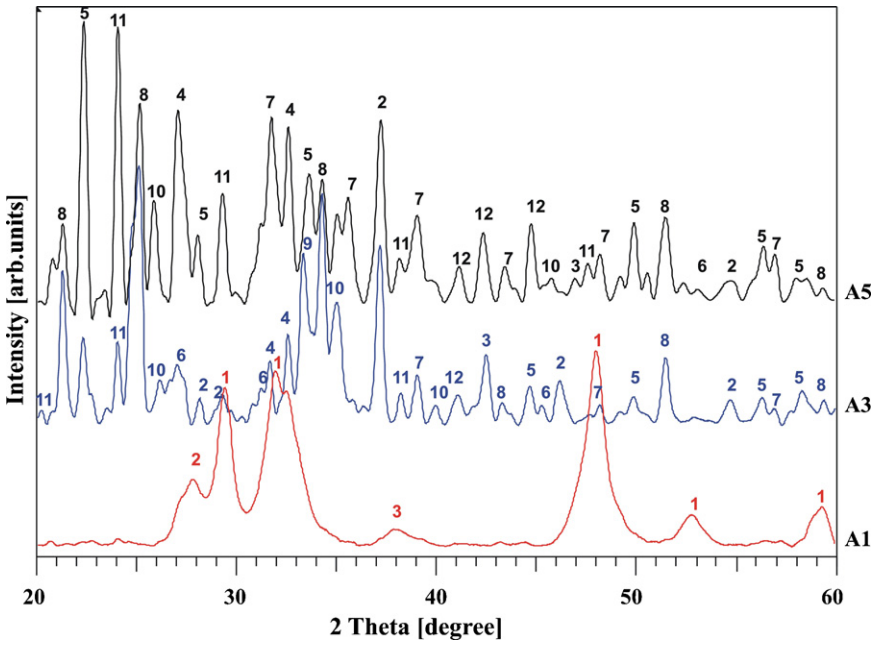

Fig. 2. The X-ray diffraction patterns of Cu_xS powders.

Table 2
The correlation between the chemical composition and photocatalytic activity of the Cu_xS samples.

Sample	$CuSO_4$: $Na_2S_2O_3$ molar ratio	Crystalline phase	Cu_xS mixture[%] (predominant Cu_xS)	MO degradation efficiency [%]	
				UV/O_2	UV/H_2O_2
A1	1	36	100 (CuS – 97%)	2.5	13
A2	5	44.5	43.7 ($Cu_{1.8}S$ – 61.8%)	9	24
A3*	10	42	43.9 ($Cu_{1.8}S$ – 50%)	16	26
A4	20	46	47 ($Cu_{1.8}S$ – 21.7%)	3	14
A5	30	45	72.5 ($Cu_{1.8}S$ – 24.5%)	1	10

* The powder further used for preparing thin films.

2 for an indirect gap semiconductor) [12]. Thus, Eq. (14) becomes Eq. (15).

$$(\alpha h\upsilon)^2 = A(h\upsilon - E_g) \quad (15)$$

The direct band gap of copper sulphide was obtained using the plots of $(\alpha h\upsilon)^2$ against $h\upsilon$ would be linear [30]. Extrapolating the straight line portion of the plot of $(\alpha h\upsilon)^2$ against $h\upsilon$, to the energy axis for zero absorption coefficient gives the optical band gap energy of the material (Fig. 3).

The value of the optical band gap of the Cu_xS film (A3 sample) was calculated at 2.1 eV, which is consistent with many literature data on copper sulphides obtained by wet chemical routes that report this value between 1.2 and 2.5 eV [31,32]. The band gap energies calculated for the Cu_xS/TiO_2 composite films were 2.37 eV (Cu_xS:TiO_2 = 1:9), 2.41 eV (Cu_xS:TiO_2 = 3:7) respectively 2.12 eV (Cu_xS:TiO_2 = 1:1), which promotes the using of solar light in a larger amount comparing to the TiO_2 thin film (band gap energy of 3.1 eV, experimentally determined).

The diagram of the charge transfer process, Fig. 4, describes the Cu_xS/TiO_2 system using the band gap energy E_g, the valence band

Table 3
The dyes degradation efficiency under UV and VIS irradiation*.

		MO photodegradation [%]				MB photodegradation [%]			
		MO/O_2		MO/H_2O_2		MB/O_2		MB/H_2O_2	
		UV	Vis	UV	Vis	UV	Vis	UV	Vis
Without catalyst		0	0	0	0	0	7	0	17
TiO_2		26	7.4	44	11.4	40	33	67	45
Cu_2S		1	0	92	10	17	0	99	37
Cu_xS/TiO_2	1:9	17.5	0	99 (300 min)	24	24	0	99	53
	3:7	17	1	99 (180 min)	62	13	0	99 (300 min)	56
	1:1	15	1	99 (240 min)	59	4	0	99 (300 min)	62

* The degradation efficiency after 6 h of irradiation, except the irradiation time listed in brackets.

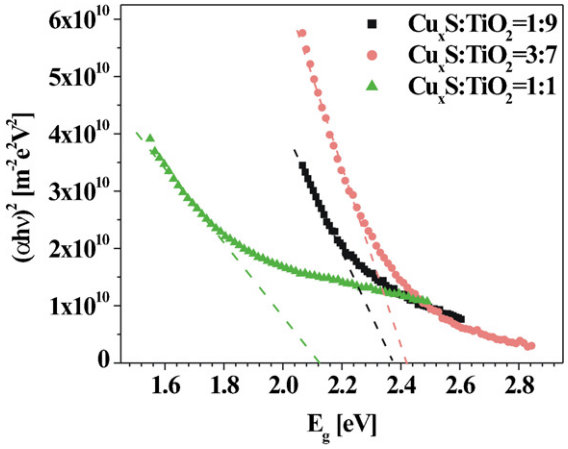

Fig. 3. The calculation of the band gap energy of the Cu_xS/TiO_2 composites films.

(VB) potential E_{VB} and the conduction band (CB) potential E_{CB} vs. normal hydrogen electrode.

One method for calculating the valence band and conduction band potentials of the semiconductors is using the following empirical equation [33]:

$$E_{VB} = \chi_{\text{semiconductor}} - E_e + 0.5E_g \quad (16)$$

where E_{VB} is the *VB* edge potential, $\chi_{\text{semiconductor}}$ is the semiconductor electronegativity, E_e is the energy of free electrons vs. hydrogen (4.5 eV), E_g is the band gap energy of the semiconductor (experimentally measured), and E_{CB} can be calculated by:

$$E_{CB} = E_{VB} - E_g \quad (17)$$

The absolute semiconductor electronegativity $\chi_{\text{semiconductor}}$ (eV) and the absolute cationic electronegativity (eV) χ_{cation} (eV) can be calculating using Eq. (18) respectively Eq. (19) where χ_{cation} (P.u.) represents the cationic electronegativity (P.u. Pauling units).

$$\chi_{\text{semiconductor}}\ (\text{eV}) = 0.45 \cdot \chi_{\text{cation}}\,(\text{eV}) + 3.36 \quad (18)$$

$$\chi_{\text{cation}}\ (\text{eV}) = \frac{\chi_{\text{cation}}(\text{P.u.}) + 0.206}{0.336} \quad (19)$$

The valence and conduction band potentials of Cu_xS and TiO_2 have been calculated using Eqs. (16)–(19) [34] and were used in Fig. 4.

Value corresponding to the valence band potential (2.73 eV) calculated for Cu_xS was close to that determined by Kashida et al. [35].

The Cu_xS and TiO_2 semiconductors have almost equal valence band potentials but significantly differ in the CB potential values, therefore in the Cu_xS/TiO_2 photocatalysts the holes and electrons were allowed to flow from a semiconductor to another, reducing the electron–hole recombination. Moreover, upon optical excitation, photo-generated electrons accumulate at the edge of the conduction band while holes accumulated at the top of the valence band. These two processes result in an enhanced efficiency of the interfacial charge-transfer towards the active species and/or towards the adsorbed dyes molecules.

3.3. The morphology of the thin films surface

The thin films surface morphology has a pronounced effect on the photocatalytic activity which is enhanced on porous structures. Atomic force microscopy images (50 μm × 50 μm) from the samples surface are shown in Fig. 5. Large area scans shows films without cracks supplementary justifying the high efficiencies in dyes photodegradation (Table 4). The images also show that the mezzo/micro particles are agglomerated in large aggregates and the distribution curves of the voids allows estimating the most likely inter-particle voids size (calculated at the half width of the peak), with almost equal values for the three samples: 2.75 ± 0.8 μm (sample A3-1), 2.5 ± 0.2 μm (sample A3-2), 2.3 ± 0.1 μm (sample A3-3).

3.4. Photocatalytic activity of the films

The activity of the films was measured based on the photocatalytic degradation efficiency of methyl orange (MO) and methylene blue (MB).

The methyl orange degradation efficiency is very low (0–5%) for Cu_xS in UV/catalyst/O_2 (air) (after 6 h of irradiation time) for the entire range of dyes concentration, increasing significantly, over 90% in diluted dye solutions, when adding H_2O_2 into the system, Fig. 6. The photodegradation activity of the catalysts in UV/H_2O_2 system was tested and the results are presented in Fig. 6 for methyl orange (Fig. 6a) and methylene blue (Fig. 6b) degradation, outlining the initial dye concentrations.

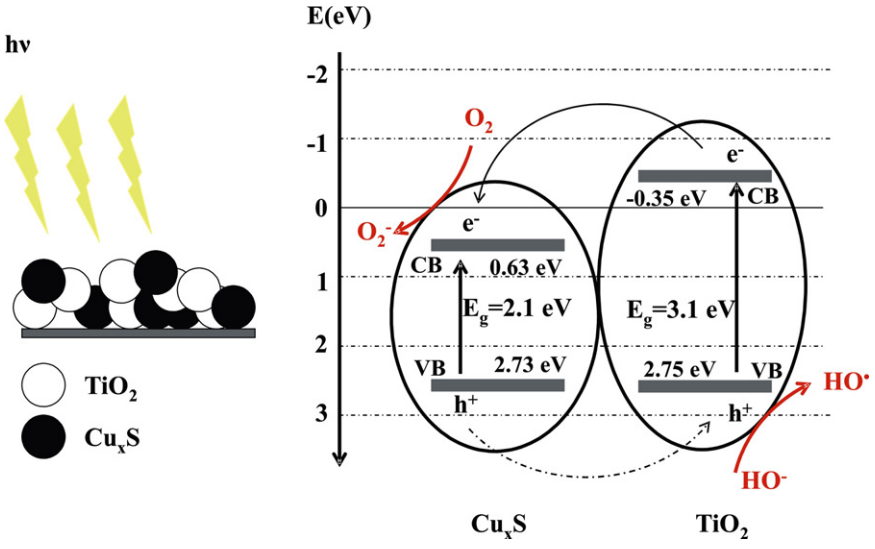

Fig. 4. Schematic diagram of charge transfer process.

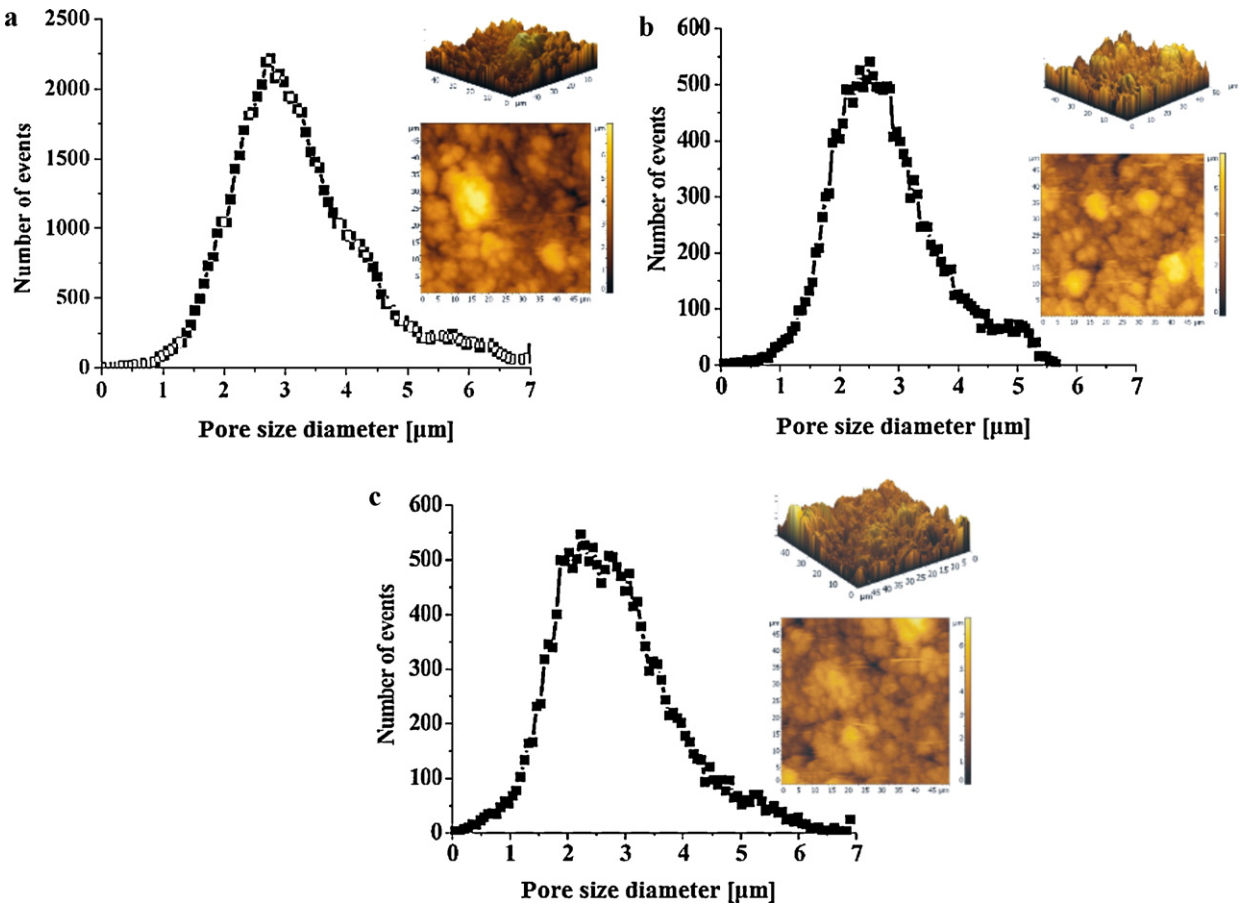

Fig. 5. The AFM topography (2D and 3D) and pore size distribution: (a) sample A3-1, (b) sample A3-2, (c) sample A3-3.

Hydrogen peroxide acts as a more efficient electron acceptor than oxygen (existent at the saturation concentration with the air, during photocatalysis, under stirring). In the UV/Cu_xS/H_2O_2 system, almost 100% of the dyes degradation was achieved within 6 h of UV irradiation indicating significantly higher values comparing to TiO_2. This effect is more pronounced in diluted solutions, both for MO and MB, when light absorption in the solutions and catalyst clogging are reduced. A complete set of investigations was thus developed on dye solutions, at concentrations of 0.0125 mM (Table 3).

The photocatalytic activity of Cu_xS/TiO_2 nanocomposites (Fig. 7 for MO respectively Fig. 8 for MB degradation) shows synergistic effects, depending on the Cu_xS:TiO_2 ratio.

Based on the data obtained under UV irradiation, further test were developed to investigate the performance of the Cu_xS/TiO_2 composite films under VIS light. The blank test shows that photo-induced self-sensitized photodegradation has little influence on the results of the experiment when only solved oxygen from air exists in the system. The preliminary results showed 1% degradation efficiency without H_2O_2 (Table 3) for both dyes.

The results can be considered promising and confirm that the semiconductors association is more efficient than its components, when an electron donor is involved. In the processes developed on the Cu_xS/TiO_2, H_2O_2 can accept an electron from the conduction band, Eq. (20), can promote charge separation forming $HO^\bullet$, Eqs. (21) and (22), and/or can react with copper cations forming additional radicals $HO_2^\bullet$ and $HO^\bullet$, Eqs. (23) and (24):

$$H_2O_2 + e^- \rightarrow HO^\bullet + HO^- \quad (20)$$

$$H_2O_2 + HO^\bullet \rightarrow H_2O + HO_2^\bullet \quad (21)$$

$$H_2O_2 + HO_2^\bullet \rightarrow H_2O + HO^\bullet + O_2 \quad (22)$$

Table 4
Langmuir–Hinshelwood kinetics parameters for the photodegradation of dyes on the Cu_xS/TiO_2 catalyst.

Dye	Electron acceptor	Catalyst	$k \cdot 10^7$ [min^{-1}]	R^2
MO	H_2O_2	Cu_xS:TiO_2 = 1:9	13.784	0.9916
		Cu_xS:TiO_2 = 3:7	25.358	0.9998
		Cu_xS:TiO_2 = 1:1	17.235	0.9829
	O_2	Cu_xS:TiO_2 = 1:9	0.511	0.9911
		Cu_xS:TiO_2 = 3:7	0.527	0.9949
		Cu_xS:TiO_2 = 1:1	0.452	0.9912
MB	H_2O_2	Cu_xS:TiO_2 = 1:9	11.922	0.9581
		Cu_xS:TiO_2 = 3:7	13.629	0.9827
		Cu_xS:TiO_2 = 1:1	14.756	0.9816
	O_2	Cu_xS:TiO_2 = 1:9	0.751	0.9912
		Cu_xS:TiO_2 = 3:7	0.164	0.9924
		Cu_xS:TiO_2 = 1:1	0.092	0.961

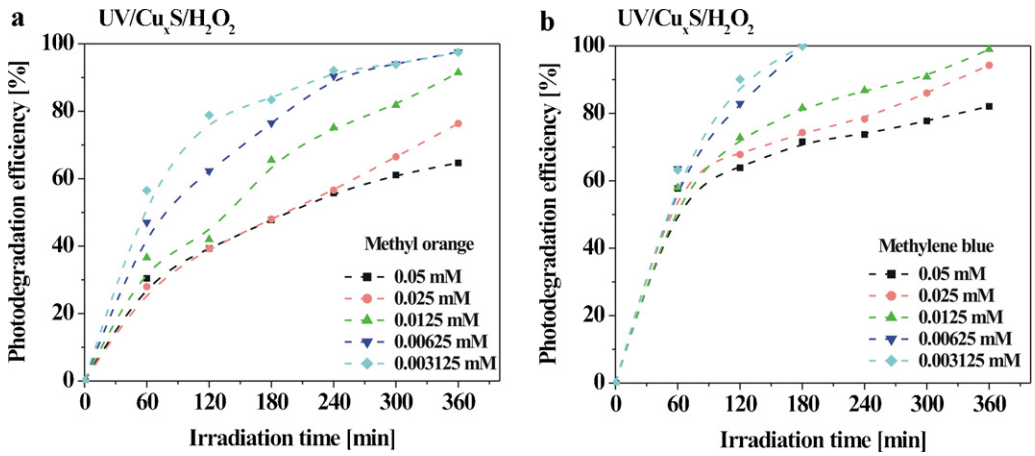

Fig. 6. Influence of the dyes concentration on the photodegradation on Cu_xS film, under UV irradiation (a) methyl orange, (b) methylene blue.

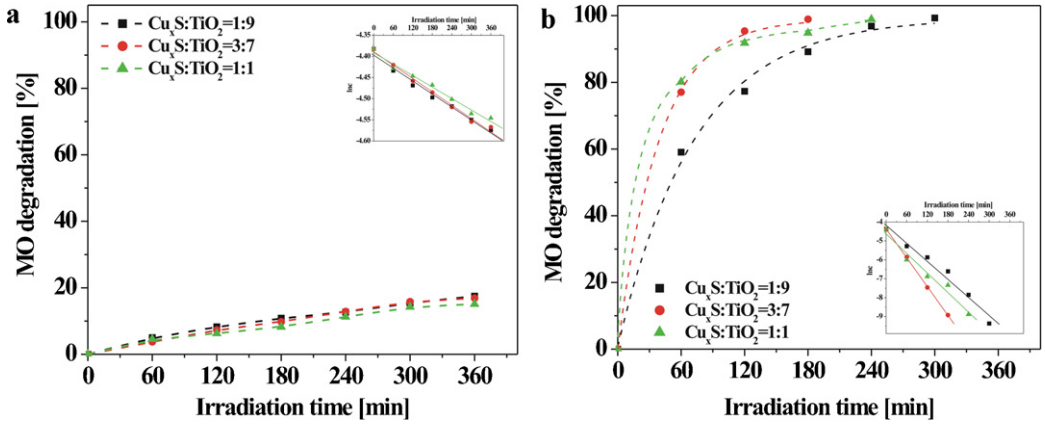

Fig. 7. Langmuir–Hinshelwood kinetics of MO degradation in (a) UV/O_2 and (b) UV/H_2O_2 systems.

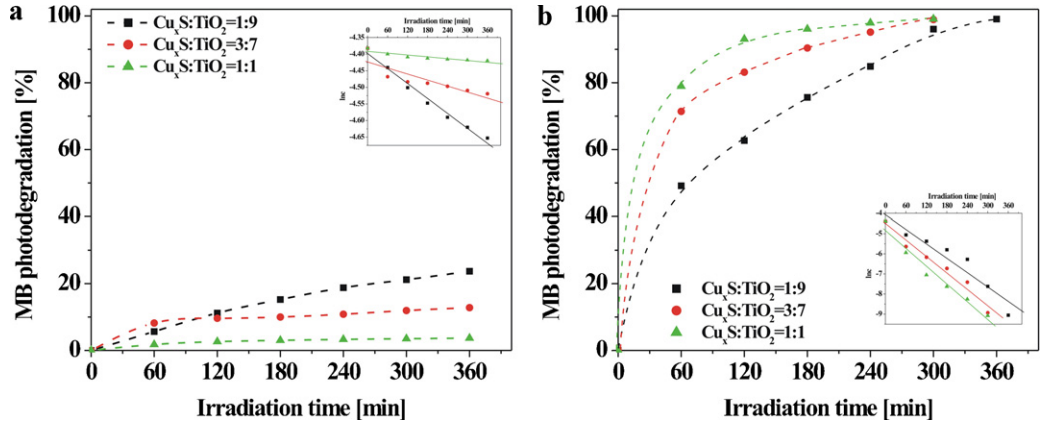

Fig. 8. Langmuir–Hinshelwood kinetics of MB degradation in (a) UV/O_2 and (b) UV/H_2O_2 systems.

$$H_2O_2 + Cu^{2+} \rightarrow HO_2^{\bullet} + H^+ + Cu^+ \quad (23)$$

$$H^+ + Cu^+ + H_2O_2 \rightarrow HO^{\bullet} + Cu^{2+} \quad (24)$$

3.5. The Langmuir–Hinshelwood kinetic

This study reports on the kinetic mechanisms, based on the experimental data of photocatalytic methyl orange (Fig. 7) and methylene blue degradation (Fig. 8), from aqueous solutions, using Cu_xS/TiO_2 catalysts, under UV irradiation (details on the mechanisms investigation under VIS light will be provided after supplementary work).

The photodegradation of dyes follows the first order reaction described by the Langmuir–Hinshelwood (L-H) mechanism [36,37]:

$$\ln c = \ln c_0 - kt \quad (25)$$

where c_0 is the initial concentration of dyes aqueous solution (mM), c is the concentration of dyes (mM) measured at the time t (min) and k is the apparent photodegradation rate constant (min^{-1}).

The selection of the optimum catalyst may be possible based on the rate constant in the photodegradation reaction (k). These values, along with the regression coefficients (R^2) of the linear fittings for dyes photodegradation are presented in Table 4.

Under similar experimental conditions, the rate constants are of similar order of magnitude (Table 4) being strongly influenced by the H_2O_2 addition, thus one may conclude that the amount of $HO^{\bullet}$ is responsible for the efficiency increase and not a change in mechanism.

As presented in Table 4, the highest MO photodegradation rate was registered on the Cu_xS:TiO_2 = 3:7 composite, when the electron acceptor (H_2O_2) was added, recommending this substrate for up scaled applications. On this catalyst, the rate constant for MB photodegradation is also reasonable high.

The kinetic characteristics of the photocatalytic degradation of dyes by a Cu_xS/TiO_2 thin film catalysts were experimentally investigated. The kinetic characteristics were ascertained to follow the Langmuir–Hinshelwood kinetic mechanism, confirming the high substrate reactivity.

4. Conclusions

This study presents the results obtained in developing new photocatalytic materials, based on copper sulphides (Cu_xS powder and film) and Cu_xS/TiO_2 nanocomposite films with enhanced degradation efficiency of dyes under UV and visible light irradiation.

The dyes degradation efficiency on copper sulphide powder is lower than on the film due to the opacity of the suspensions. In these conditions, the penetration depth of the photons is decreased and less catalysts nanoparticles could be activated.

The higher activity of Cu_xS/TiO_2 composites compared with the activity of Cu_xS and of TiO_2 is explained by the irreversible charge separation, decreasing the kinetic constraints when interacting with the dye pollutants.

The photocatalytic experiments demonstrated that the Cu_xS/TiO_2 hybrid photocatalysts activated with H_2O_2 exhibited a higher catalytic efficiency (99%) for dyes degradation comparing to the mono-component films. Moreover, the preparation method should also be able to be extended to the synthesis of other similar coupled metal sulphide and oxide hybrid photocatalysts.

Acknowledgements

This paper is supported by the Sectoral Operational Programme Human Resources Development (SOP HRD), financed from the European Social Fund and by the Romanian Government under the contract number POSDRU ID59323.

References

[1] S. Malato, P. Fernández-Ibáñez, M. Maldonado, J. Blanco, W. Gernjak, Decontamination and disinfection of water by solar photocatalysis: recent overview and trends, Catal. Today 147 (2009) 1–59.
[2] O. Prieto, J. Fermoso, Y. Nuñez, J.L. del Valle, R. Irusta, Decolouration of textile dyes in wastewaters by photocatalysis with TiO_2, Sol. Energy 79 (2005) 376–383.
[3] K. Rajeshwar, M.E. Osugi, W. Chanmanee, C.R. Chenthamarakshan, M.V.B. Zanoni, P. Kajitvichyanukul, R. Krishnan-Ayer, Heterogeneous photocatalytic treatment of organic dyes in air and aqueous media, J. Photochem. Photobiol. C 9 (2008) 171–192.
[4] S.K. Kansal, M. Singh, D. Sud, Studies on photodegradation of two commercial dyes in aqueous phase using different photocatalysts, J. Hazard. Mater. 141 (2007) 581–590.
[5] A. Martínez-de la Cruz, D.S. Martínez, E.L. Cuéllar, Synthesis and characterization of WO_3 nanoparticles prepared by the precipitation method: evaluation of photocatalytic activity under vis-irradiation, Solid State Sci. 12 (2010) 88–94.
[6] M. Muruganandham, I.S. Chen, J.J. Wu, Effect of temperature on the formation of macroporous ZnO bundles and its application in photocatalysis, J. Hazard. Mater. 172 (2009) 700–706.
[7] J.M. Herrmann, C. Duchamp, M. Karkmaz, B.T. Hoai, H. Lachheb, E. Puzenat, C. Guillard, Environmental green chemistry as defined by photocatalysis, J. Hazard. Mater. 146 (2007) 624–629.
[8] J. Li, J.Z. Zhang, Optical properties and applications of hybrid semiconductor nanomaterials, Coord. Chem. Rev. 253 (2009) 3015–3041.
[9] Y. Bessekhouad, D. Robert, J. Weber, Bi_2S_3/TiO_2 and CdS/TiO_2 heterojunctions as an available configuration for photocatalytic degradation of organic pollutant, J. Photochem. Photobiol. A 163 (2004) 569–580.
[10] B. Pourabbas, B. Jamshidi, Preparation of MoS_2 nanoparticles by a modified hydrothermal method and the photo-catalytic activity of MoS_2/TiO_2 hybrids in photo-oxidation of phenol, Chem. Eng. J. 138 (2008) 55–62.
[11] D. Jing, L. Guo, WS_2 sensitized mesoporous TiO_2 for efficient photocatalytic hydrogen production from water under visible light irradiation, Catal. Commun. 8 (2007) 795–799.
[12] F. Zhuge, X. Li, X. Gao, X. Gan, F. Zhou, Synthesis of stable amorphous Cu_2S thin film by successive ion layer adsorption and reaction method, Mater. Lett. 63 (2009) 652–654.
[13] A.A. Sagade, R. Sharma, Copper sulphide (Cu_xS) as an ammonia gas sensor working at room temperature, Sensor Actuators B 133 (2008) 135–143.
[14] M.A. Zhukovskiy, A.L. Stroyuk, V.V. Shvalagin, N.P. Smirnova, O.S. Lytvyn, A.M. Eremenko, Photocatalytic growth of CdS, PbS, and Cu_xS nanoparticles on the nanocrystalline TiO_2 films, J. Photochem. Photobiol. A 203 (2009) 137–144.
[15] S.Y. Wang, W. Wang, Z.H. Lu, Asynchronous-pulse ultrasonic spray pyrolysis deposition of Cu_xS (x = 1, 2) thin films, Mater. Sci. Eng. B 103 (2003) 184–188.
[16] E.N. Selivanov, R.I. Gulyaeva, A.D. Vershinin, Thermal expansion and phase transformations of copper sulfides, Inorg. Mater. 43 (2007) 573–578.
[17] L. Isac, A. Duta, A. Kriza, S. Manolache, M. Nanu, Copper sulfides obtained by spray pyrolysis—possible absorbers in solid-state solar cells, Thin Solid Films 515 (2007) 5755–5758.
[18] S. Gorai, D. Ganguli, S. Chaudhuri, Shape selective solvothermal synthesis of copper sulphides: role of ethylenediamine–water solvent system, Mater. Sci. Eng. B 116 (2005) 221–225.
[19] J. Zou, J. Zhang, B. Zhang, P. Zhao, K.X. Huang, Low-temperature synthesis of copper sulfide nano-crystals of novel morphologies by hydrothermal process, Mater. Lett. 61 (2007) 5029–5032.
[20] J.N. Solanki, R. Sengupta, Z.V.P. Murthy, Synthesis of copper sulphide and copper nanoparticles with microemulsion method, Solid State Sci. 12 (2010) 1560–1566.
[21] S.K. Mathew, N.P. Rajesh, M. Ichimura, Udayalakshmi, Preparation and characterization of copper sulfide particles by photochemical method, Mater. Lett. 62 (2008) 591–593.
[22] J. Podder, R. Kobayashi, M. Ichimura, Photochemical deposition of Cu_xS thin films from aqueous solutions, Thin Solid Films 472 (2005) 71–75.
[23] M. Visa, C. Bogatu, A. Duta, Simultaneous adsorption of dyes and heavy metals from multicomponent solutions using fly ash, Appl. Surf. Sci. 256 (2010) 5486–5491.
[24] I. Horcas, R. Fernandez, J.M. Gomez-Rodriguez, J. Colchero, J. Gomez-Herrero, A.M. Baro, WSxM: a software for scanning probe microscopy and a tool for nanotechnology, Rev. Sci. Instrum. 78 (2007), 013705-113705.
[25] L. Andronic, A. Duta, The influence of TiO_2 powder and film on the photodegradation of methyl orange, Mater. Chem. Phys. 112 (2008) 1078–1082.
[26] P.K. Nair, J. Cardoso, O. Gomez Daza, M.T.S. Nair, Polyethersulfone foils as stable transparent substrates for conductive copper sulfide thin film coatings, Thin Solid Films 401 (2001) 243–250.
[27] Y. Rodríguez-Lazcano, H. Martinez, M. Calixto-Rodriguez, A. Nunez Rodriguez, Properties of CuS thin films treated in air plasma, Thin Solid Films 517 (2009) 5951–5955.
[28] K.M. Gadave, C.D. Lokhande, Formation of Cu_xS films through a chemical bath deposition process-letter, Thin Solid Films 229 (1993) 1–4.
[29] C. Yang, H. Fan, Y. Xi, J. Chen, Z. Li, Effects of depositing temperatures on structure and optical properties of TiO_2 film deposited by ion beam assisted electron beam evaporation, Appl. Surf. Sci. 254 (2008) 2685–2689.
[30] H.M. Pathan, J.D. Desai, C.D. Lokhande, Modified chemical deposition and physico-chemical properties of copper sulphide (Cu_2S) thin films, Appl. Surf. Sci. 202 (2002) 47–56.
[31] S.D. Sartale, C.D. Lokhande, Growth of copper sulphide thin films by successive ionic layer adsorption and reaction (SILAR) method, Mater. Chem. Phys. 65 (2000) 63–67.
[32] S.V. Bagul, S.D. Chavhan, R. Sharma, Growth and characterization of Cu_xS (x = 1.0 1. 76, and 2. 0) thin films grown by solution growth technique (SGT), J. Phys. Chem. Solids 68 (2007) 1623–1629.
[33] C. Gao, J. Li, Z. Shan, F. Huang, H. Shen, Preparation and visible-light photocatalytic activity of In_2S_3/TiO_2 composite, Mater. Chem. Phys. 122 (2010) 183–187.
[34] C.W. Kwon, A. Poquet, S. Mornet, G. Campet, M.H. Delville, M. Treguer, J. Portier, Electronegativity and chemical hardness: two helpful concepts for understanding oxide nanochemistry, Mater. Lett. 51 (2001) 402–413.
[35] S. Kashida, W. Shimosaka, M. Mori, D. Yoshimura, Valence band photoemission study of the copper chalcogenide compounds, Cu_2S, Cu_2Se and Cu_2Te, J. Phys. Chem. Solids 64 (2003) 2357–2363.
[36] N. Guettaï, H. Ait Amar, Photocatalytic oxidation of methyl orange in presence of titanium dioxide in aqueous suspension. Part II: kinetics study, Desalination 185 (1–3) (2005) 439–448.
[37] K.V. Kumar, K. Porkodi, F. Rocha, Langmuir–Hinshelwood kinetics––a theoretical study, Catal. Commun. 9 (2008) 82–84.